Artificial Magnetic Tripod Ice

Xiaoyu Zhang,[1,*] Ioan-Augustin Chioar,[1,*] Grant Fitez,[2] Anthony Hurben,[1] Michael Saccone,[3] Nicholas S. Bingham,[1,†] Justin Ramberger,[4] Chris Leighton,[4] Cristiano Nisoli,[3] and Peter Schiffer[1,2,‡,§]

[1]*Department of Applied Physics, Yale University, New Haven, Connecticut 06511, USA*
[2]*Department of Physics, Yale University, New Haven, Connecticut 06511, USA*
[3]*Theoretical Division and Center for Nonlinear Studies, Los Alamos National Laboratory, Los Alamos, New Mexico 87545, USA*
[4]*Department of Chemical Engineering and Materials Science, University of Minnesota, Minneapolis, Minnesota 55455, USA*

(Received 17 May 2023; accepted 10 August 2023; published 19 September 2023)

We study the collective behavior of interacting arrays of nanomagnetic tripods. These objects have six discrete moment states, in contrast to the usual two states of an Ising-like moment. Our experimental data demonstrate that triangular lattice arrays form a "tripod ice" that exhibits charge ordering among the effective vertex magnetic charges, in direct analogy to artificial kagome spin ice. The results indicate that the interacting tripods have effective moments that act as emergent local variables, with strong connections to the well-studied Potts and clock models. In addition, the tripod moments display a tendency toward a nearest neighbor alignment in our thermalized samples that separates this system from kagome spin ice. Our results open a path toward the study of the collective behavior of nonbinary moments that is unavailable in other physical systems.

DOI: 10.1103/PhysRevLett.131.126701

The nanomagnet arrays known collectively as artificial spin ice have offered an important window into collective behavior associated with frustrated interactions. The ability to both design the array structures and probe the resultant moment configurations microscopically has revealed a disparate class of phenomena, including topological excitations, effective magnetic monopoles, and various types of ordering [1–3].

The elementary magnetic degree of freedom in existing artificial spin ices has most typically been an Ising-like binary moment associated with a single-domain ferromagnetic nanomagnet. Experimentally, this has been most commonly realized as a stadium-shaped island or a wire, so that shape anisotropy aligns the moment with the geometric long axis [4,5], or a disc with perpendicular magnetic anisotropy [6,7]. Other groups have examined circular islands to allow for XY symmetry [8–10], or deployed either rectangular islands [11] or closely-paired stadium-shaped islands [12], both of which create effective quadrupole moments. In each case, the fundamental elements have direct counterparts in atomic magnetic moments.

In this work, we examine an alternative fundamental building block, the magnetic tripod, in which the nanomagnet structure has threefold symmetry and six possible effective moment states. We experimentally investigate interacting tripods placed on a triangular lattice, allowing comparison with the classic kagome structure. Our results demonstrate that this tripod ice displays qualitatively distinct collective behavior and suggest a panoply of new physics in different geometries of tripod arrays.

Our tripods are threefold-symmetric Y-shaped ferromagnetic nanoislands, as illustrated in Fig. 1. The tripods are arranged in a regular triangular lattice array, which we call "triangular tripod ice" in analogy to naming conventions for other artificial spin ice systems. We placed the tripods with identical orientations in this initial study, choosing one of the simplest possible structures that reflects the threefold symmetry of the tripods. This geometry has the advantage that it is directly comparable to the conventional kagome ice lattice (the triangular tripod lattice can be formed by connecting every other vertex of the kagome structure). Our structure therefore allows us to elucidate what new physics arises from having tripods as the fundamental unit, as opposed to separated triads of stadium-shaped nanomagnets each behaving as a dipole.

Our permalloy structures had thickness of 15 nm, and were defined by the lattice constant a, the leg length r, and leg width w, where all parameters are defined in Fig. 1(f). We parametrize the samples in terms of the gap between the tripods ($g = a - r$), since the interaction is strongly correlated with gap size, and we focus on samples with dimensions of $r = 220$ nm, $w = 80$ nm, and varying values of a (resulting in $g = 30$–300 nm). A second set of samples with $r = 160$ nm and $w = 60$ nm showed qualitatively similar behavior. The magnetic state of the lattice was measured with magnetic force microscopy (MFM) after each sample was thermalized by heating to slightly above the Curie temperature for permalloy and cooling slowly, allowing the moments to reach a low-energy collective state [13]. Details of sample deposition, lithography, and thermalization are given in the Supplemental Material [14]. For comparison, we also studied two kagome spin ice samples with isolated islands of dimension 220 nm × 80 nm and lattice parameters of 320 and 360 nm, which were grown simultaneously on the

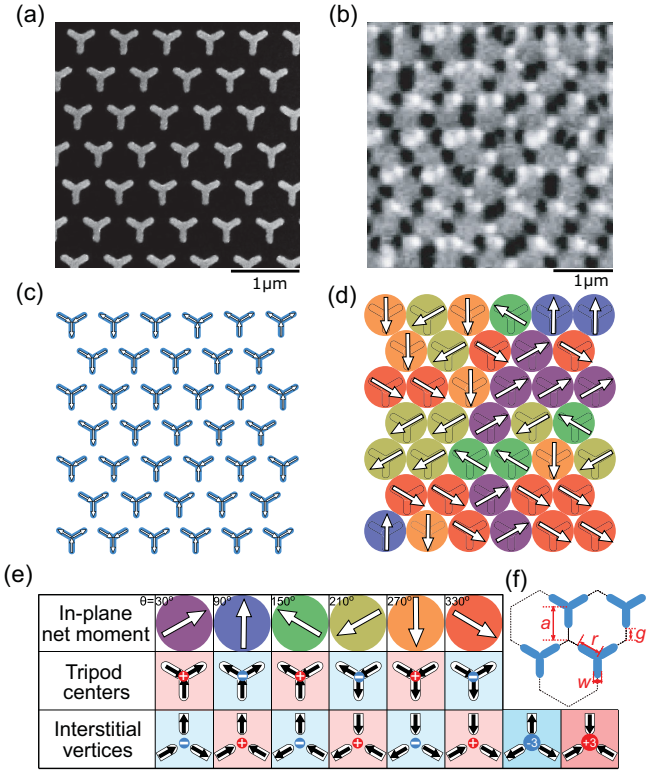

FIG. 1. Magnetic tripod lattice. (a) Scanning electron microscopy image of triangular tripod ice with $g = 140$ nm. (b) Magnetic force microscopy image of the same sample. (c) Map of the moments of the individual legs from the MFM image. (d) Map of the tripod moments from the MFM image. (e) Top row: color scheme for the six possible tripod states, with the arrows indicating the effective tripod moment direction. Middle row: Magnetic charges at the tripod centers, with arrows indicating the dipole moments of the legs. Bottom row: Magnetic charges at the interstitial vertices between tripods, with arrows indicating the dipole moments of the legs. (f) Schematic of the tripod lattice, indicating the lattice constant a, the length of each leg r, the leg width w, and the gap g.

same substrate. (A schematic of the kagome ice lattice parameter is shown in the Supplemental Material [14]).

The MFM images, such as shown in Fig. 1(b), demonstrate that the tip of each of the three legs of each tripod has either a north or south magnetic pole, so that the three points of each island each have a magnetic pole (and a fourth magnetic pole is at the center of each structure). We note that the domain structures of similar-shaped (but larger) magnetic objects were examined previously, and those showed both complex magnetic domains as well as the simple three-pole state that we observe, depending on the interactions [25,26]. Micromagnetics also confirm that the directions of the leg dipole moments obey the ice rule, with two pointing in and one out, or vice versa (see Supplemental Material [14]). If one considers each leg dipole as having an effective magnetic charge of $q = \pm 1$ at each end, the tripod has those effective charges at the ends of each of its three legs, and an effective net charge of ± 1 at the center, associated with a domain wall. These charges are illustrated in Fig. 1(e), along with the charges of ± 1 or ± 3 at the interstitial points.

As noted above, because the legs of the tripods are on the edges of a kagomelike lattice, the moments of the legs can be easily mapped onto the moment structure of the well-studied kagome ice geometry [2,3,5,27–29]. Unlike kagome ice, however, there is a symmetry breaking between the tripod centers and the interstitial vertices of the tripod lattice. The kagome ice vertices on the tripod centers are always connected, whereas on the interstitial vertices the islands are separated by the gaps, as illustrated in Fig. 1(f). In the limit of $g = 0$, the symmetry breaking is removed, and the system becomes equivalent to a connected kagome ice [30,31], which experimentally shows a low energy state very similar to kagome ice composed of isolated islands. The collective dynamics of connected artificial spin ice is associated with domain wall motion through the structure [32], as opposed to individual moment reversals, and is thus quite different from the isolated tripods we are examining.

Because of the symmetry breaking, we model tripod ice by defining a new nonbinary variable, the tripod moment m, which aligns with the combined net dipole moment of the three legs and is designated by its orientation, θ. We note that θ has six possible values, as shown in Fig. 1(e) (top row). Thus, m can be considered a six-state Potts variable [33,34], or, equivalently, a clock variable. Potts variables and Potts model Hamiltonians have been the subject of theoretical studies since the 1950s, when they were introduced as a generalization of the Ising model, and have since found applications ranging from magnetism [35], including artificial spin ice [11,12], to computational biology [36,37] and complex networks [38]. We are unaware, however, of previous experimental systems in which a six-state Potts variable has been examined in detail. We also note that the thermal magnetic reversal processes of these structures are likely to be constrained to rotate m in increments of 60 degrees when a single leg domain flips orientation, thus putting interesting constraints on the dynamics.

We now turn to the statistics of the measured magnetic configurations, obtained from the MFM images of our thermalized arrays. We first perform a comparison to expectations for the thoroughly examined kagome ice system [2,27,30,39,40]. By mapping the tripod charges onto a kagome ice structure, we find a configuration exhibiting crystallites of charge ordering among the magnetic charges on the tripod centers and interstitial vertices. This is demonstrated in Fig. 2(c), where we show an example of real-space charge ordering from one of our MFM scans. We note that these data are qualitatively similar to charge crystallites observed experimentally in thermalized kagome ice, which reproducibly are near the

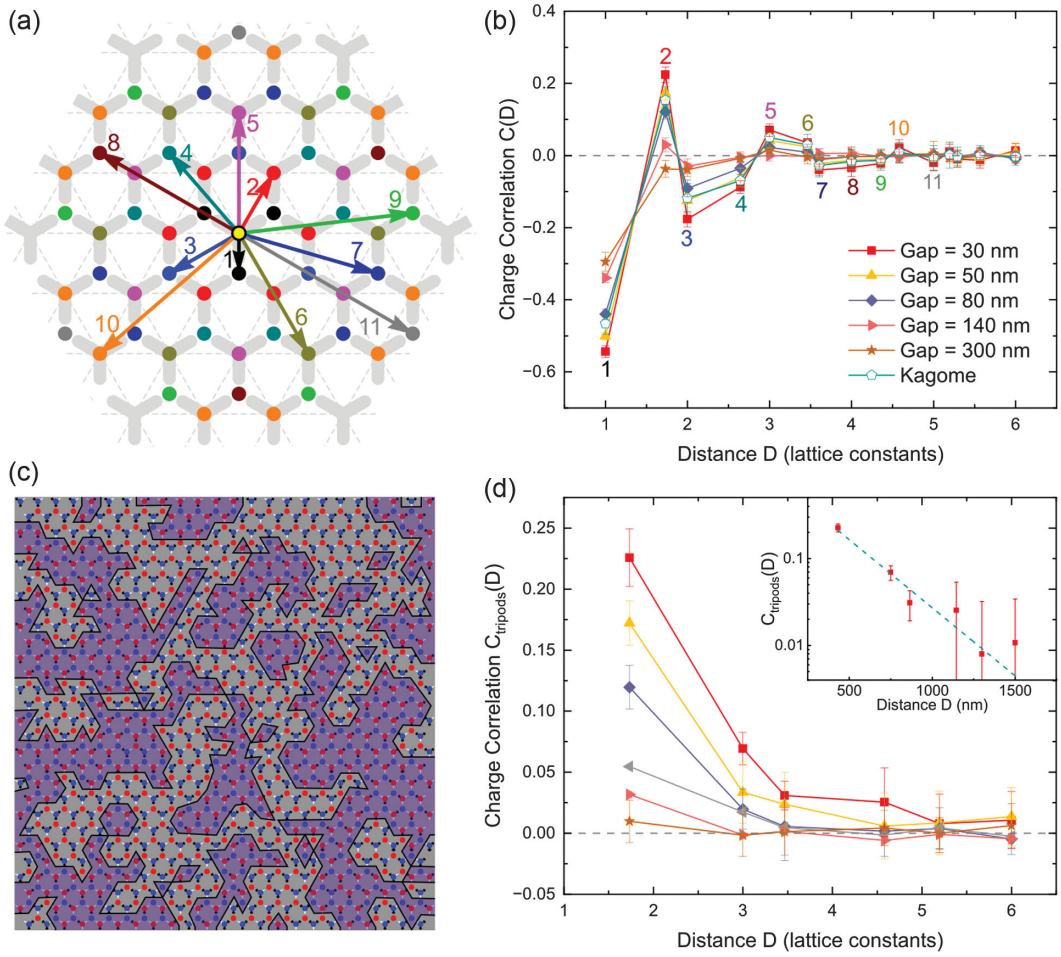

FIG. 2. Charge correlations. (a) Schematic showing the charge-charge distance order between tripod centers and interstitial vertices, labeled by increasing neighbor distance. (b) The charge correlation as a function of vertex separation and comparison with the result from our measurement of the 320 nm kagome ice. (c) A typical map of the magnetic charges in tripod ice from an MFM image. Crystallites of charge ordering are shaded grey and purple, and the charges at the tripod centers and interstitial vertices indicated with red and blue dots. The image was taken from the $g = 30$ nm array. (d) The charge correlation between the tripod centers as a function of distance. The inset shows the data for the $g = 30$ nm array on a semilog scale, suggesting an exponential dependence. The error bars in (b) and (d) are the standard error from multiple MFM images.

Ice-II transition and in good agreement with Monte Carlo calculations [28–31,41,42].

To further analyze our observed charge ordering, in Fig. 2(b) we plot the charge correlation vs the separation between charges (D), with the neighbor distances illustrated in Fig. 2(a). The charge correlation is defined as $C(D) = \langle q_i q_j \rangle$, where q_i and q_j have distance D between all effective magnetic charges on both the tripod centers and the interstitial center points between tripods. For comparison, we also plot the charge correlations from our measurements of kagome ice, and the agreement is striking.

Figure 2(d) shows the correlation of charges just on the tripod centers, $C_{\text{tripod}}(D)$, demonstrating that those correlations decrease monotonically with separation on the lattice, and that there is strong dependence on the gap size. The inset to Fig. 2(d) shows that, in the case of the strongest correlation ($g = 30$ nm), the charge correlation has an apparent exponential decay with distance, with a fit that indicates a decay length of 277 ± 7.4 nm. The exponential decay suggests equilibration just above the charge ordering transition [28,41], where charge correlations are expected to decay exponentially with a correlation length diverging at the transition. Our kagome ice data in Fig. 2(b) show similar exponential behavior over the limited range in which we have results. To the best of our knowledge, experimental observation of such behavior has not been previously reported for artificial spin ices.

Having compared the charge correlations with the kagome structure, we now consider the correlations among the effective magnetic moments associated with the tripods. Figure 3 shows the correlation $M(D) = \langle m_i \cdot m_j \rangle$ among neighboring tripods, versus their separation distance. We see a clear correlation among nearest-neighbor tripods, which decays rapidly with separation. The positive value of M for the closest spacing suggests that there is a net effective ferromagnetic interaction between neighboring

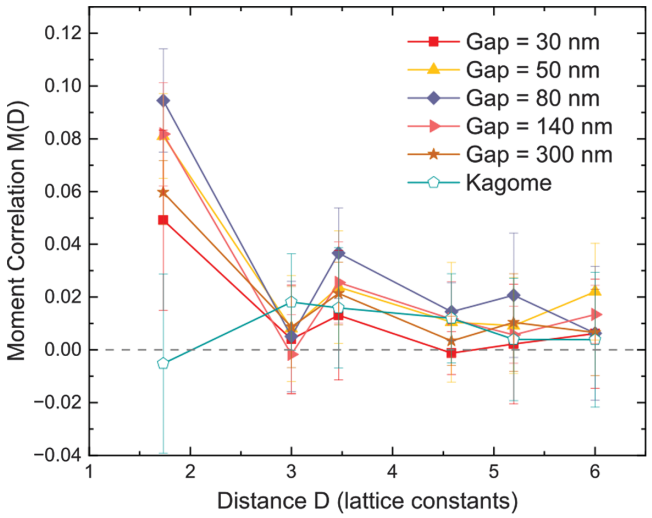

FIG. 3. Tripod moment correlations. The moment correlation for various tripod ice lattices as a function of distance between the tripod moments. The equivalent for the 320 nm kagome ice is also shown. The error bars are the standard error from multiple MFM images.

tripod moments. In the same figure, we compare with the equivalent correlations from our measurements of the 320 nm kagome ice, extracted by ascribing to every other vertex in the kagome ice structure a net moment with six possible directions, as described in Supplemental Material [14]. The much larger value of the nearest neighbor M for the tripod ice samples compared with the kagome ice samples indicates that the tripod ferromagnetic correlation is not due to the small background magnetic field that is present during thermalization. Furthermore, the measured correlation demonstrates that the tripod ice system has novel collective behavior that is associated with the tripod as a fundamental building block.

In Fig. 4 we examine the gap dependence of nearest-neighbor charge and effective tripod moment correlations for both sets of tripod ice samples, using the gap as a tuning parameter for the strength of the pairwise tripod interactions. We also compare with results from Metropolis Monte Carlo simulations of dipolar kagome ice [43], mapping each gap value to an effective temperature determined by minimizing the overall difference between the experimental and simulated charge correlations for different neighbors (as described in the Supplemental Material [14]). In Fig. 4(a), we see that the charge correlations track almost perfectly between tripod ice and kagome ice [as might have been expected from Fig. 2(b)], validating the choice of the charge correlators for bridging between the two structures. By contrast, there is a striking difference in the development of the nearest-neighbor tripod moment correlations [Fig. 4(b)], where the kagome ice tripod moment correlation is determined as described above for Fig. 3. This affirms that the tripod moments have a net positive correlation with each other, which distinguishes them from the kagome system. We note

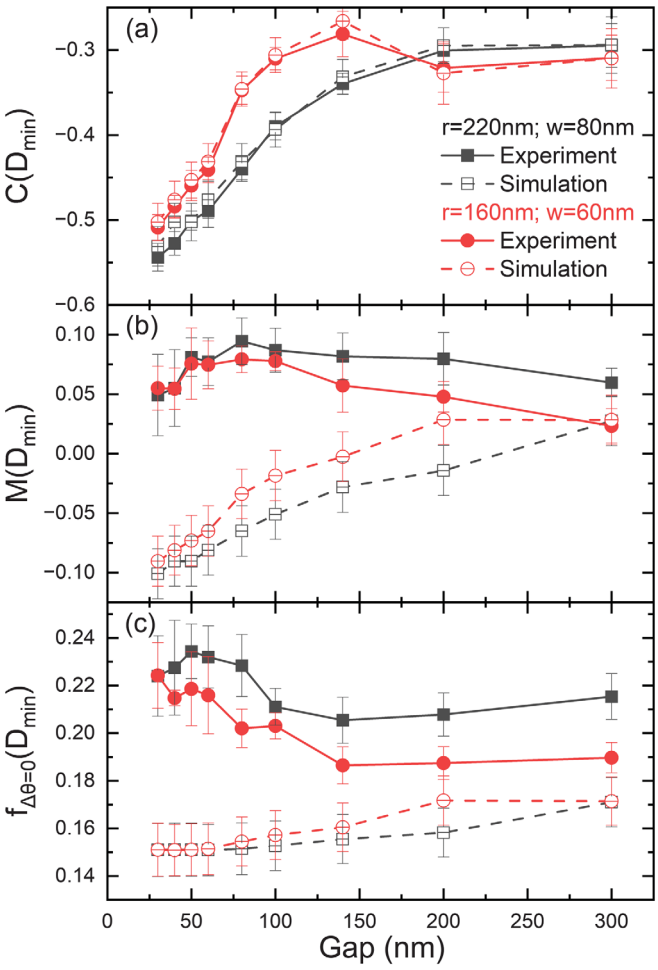

FIG. 4. Gap dependence of correlations. Various measures of correlations for nearest neighbors ($D_{\min}$) in triangular tripod ice (experimental data) and kagome ice (simulations). Note that $D_{\min}$ has a different definition for the different quantities plotted. (a) The charge correlation $C(D_{\min})$. (b) The tripod moment correlation $M(D_{\min})$. (c) The fraction of nearest neighbors with the same effective moment orientation $f_{\Delta\theta=0}(D_{\min})$. Data are shown for both shapes of tripods studied and for Monte Carlo simulations of the dipolar kagome ice system. The value of the gap used for the kagome simulation data is obtained as described in the text. The error bars are the standard error from all MFM images.

that the Monte Carlo values for dipolar kagome ice are lower than those observed experimentally for the kagome ice system in Fig. 3, possibly due to a small background magnetic field during thermalization or lack of full ergodicity in the thermalization process.

We further explore the nearest neighbor ferromagnetic correlations among the tripod moment by defining the fraction of neighboring tripods with angular differences between their moments of $\Delta\theta = \theta_i - \theta_j = 0$. We define this correlated fraction as

$$f_{\Delta\theta=0}(D) = \frac{\text{Total number of } (m_i, m_j) \text{ pairs when } m_i m_j \text{ align}}{\text{Total number of } (m_i, m_j) \text{ pairs}}$$

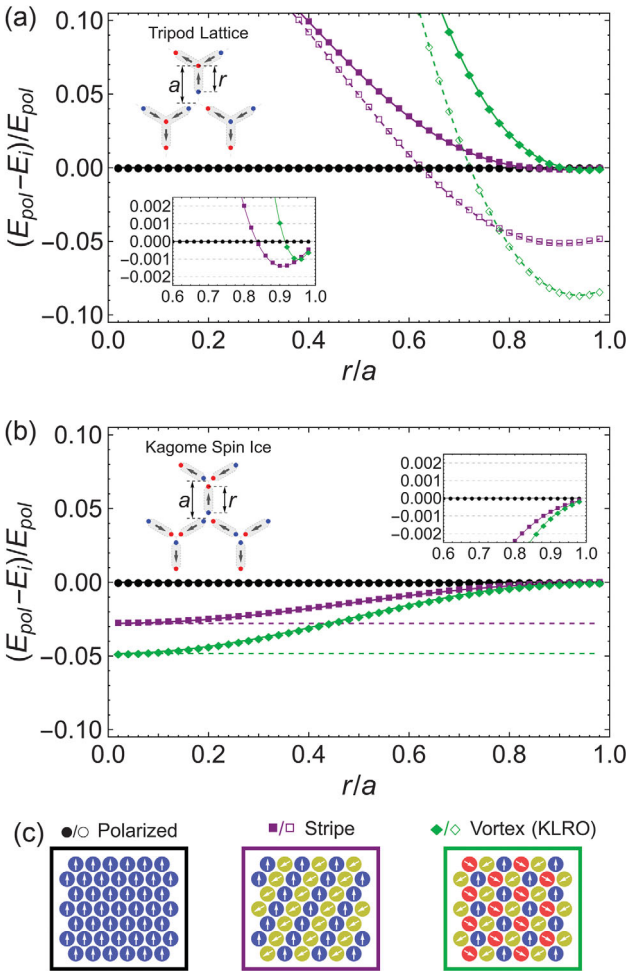

FIG. 5. Energetics of ordered states of tripod ice. Relative energy differences with respect to a polarized state for different magnetic textures as a function of leg length ratio r/a. (a) Data for a magnetic tripod lattice. (b) Data for a dipolar kagome spin ice lattice. (c) Color-coded schematics of three possible ground state candidates: black for polarized state, violet for stripe state, and green for vortex state (equivalent to the kagome long-range-ordered state). The filled symbols with solid lines are calculated using the Coulomb interaction model and open symbols with dashed lines are calculated employing the point dipole approximation. The insets give magnified plots around $r/a \approx 1$.

as a function of the distance D between the tripod centers of m_i and m_j. For a random distribution of moments, $f_{\Delta\theta=0}$ should be $1/6$, and we see that the data are well above that value, indicating a tendency for alignment of neighboring tripod moments. We note that $f_{\Delta\theta=0}$ is a different measure from M, since $f_{\Delta\theta=0}$ measures whether neighboring pairs have exactly the same tripod moment or not. The values of $f_{\Delta\theta=0}$ greater than $1/6$ in Fig. 4(c) suggests that the low energy state of the system has effective ferromagnetic nearest neighbor interactions among the tripod moments, again confirming the difference with dipolar kagome ice, and indicating that the tripod collective behavior is qualitatively different.

Since the ground state of dipolar kagome ice was somewhat complex to ascertain originally [28,41,44], and we expect a similar near degeneracy of multiple states in tripod ice, we consider possible low-energy states of the tripod ice system without definitively identifying a ground state. Toward that end, we examine the dependence of the system energy on the ratio of the leg length to the lattice parameter, i.e., r/a, both within a Coulomb description and a point dipole description as shown in Figs. 5(a) and 5(b) (see Supplemental Material [14] for details). Specifically, we examined simple ordered states of the tripod moments in which the charges are also ordered, choosing a polarized (ferromagnetic) state, a stripe state, and a vortex state that corresponds to the ordered ground state of dipolar kagome ice drawn in Fig. 5(c). As seen in Fig. 5(a), the polarized state is the lowest in energy, except for larger values of r/a, where the energy hierarchy between the considered magnetic configurations displays a high sensitivity to this ratio. This contrasts sharply with the same calculation for the kagome lattice in Fig. 5(b), for which the vortex state has the lowest energy (as expected from previous work [28,41]). The ferromagnetic correlations between nearest-neighbor tripod moments in Figs. 4(b) and 4(c), as well as the nonmonotonic behavior in M as a function of gap size, are consistent with the tendency for a polarized state in close energetic proximity to other ordered states. We note that minor lithographic imperfections in the experimental structures will also affect the superparamagnetic freezing of the system in any thermalization process, further obscuring the range of possible ground states for the structure.

The combination of the results in Figs. 3–5 demonstrate that interacting tripods, each representing sixfold Potts states, have collective behavior that is fundamentally different from Ising-like stadium-shaped moments used in the preponderance of previous artificial spin ice studies. While we only explored one of the simplest possible lattices, our demonstration opens the door for exploring potentially novel spin textures and collective spin dynamics in mesoscopic magnetic architectures, beyond the Ising framework. Unlike the quadrupolar units created previously in square islands or pairs of stadium-shaped islands [11,12], this system is comprised of building blocks with a fundamental symmetry that has no obvious previous experimental analog either in artificial spin systems or atomic magnetic structures. We expect that the tripods can be combined into a wide range of lattices to realize a variety of new frustrated systems, including hybrid behavior that combines Ising states with Potts states. The advent of tripod systems also opens the possibility of experimentally exploring collective behavior of such magnetic elements, e.g., by incorporating real-time XMCD-PEEM imaging to study the dynamics of Potts states, offering novel vistas for exploring previously inaccessible statistical mechanical properties.

Work at Yale University was funded by the U.S. Department of Energy (DOE), Office of Basic Energy

Sciences, Materials Sciences and Engineering Division under Grant No. DE-SC0020162. Work at the University of Minnesota was supported by NSF through Grant No. DMR-2103711. The work of C. N. and M. S. was carried out under the auspices of the U.S. DOE through LANL, operated by Triad National Security, LLC (Contract No. 892333218NCA000001) and financed by DOE LDRD. We are grateful to N. Strandqvist for helpful conversations. J. R. performed film depositions under the guidance of C. L., with X. Z., N. S. B. and A. H. overseeing the lithography. X. Z. and N. S. B. performed the MFM measurements. X. Z., I.-A. C., G. F., and M. S. analyzed the data. I.-A. C. performed the Monte Carlo simulations and energy calculations. C. N. contributed to theoretical interpretations. P. S. supervised the entire project. All authors contributed to the discussion of results and to the finalization of the manuscript.

[*]These authors contributed equally to this work.
[†]Current address: Department of Physics, University of Maine, Orono, Maine 04469, USA.
[‡]Current address: Department of Physics, Princeton University, Princeton, NJ 08540 USA.
[§]pschiffer@princeton.edu

[1] I. Gilbert, C. Nisoli, and P. Schiffer, Frustration by design, Phys. Today **69**, No. 7, 54 (2016).
[2] S. H. Skjærvø, C. H. Marrows, R. L. Stamps, and L. J. Heyderman, Advances in artificial spin ice, Nat. Rev. Phys. **2**, 13 (2020).
[3] P. Schiffer and C. Nisoli, Artificial spin ice: Paths forward, Appl. Phys. Lett. **118**, 110501 (2021).
[4] R. F. Wang *et al.*, Artificial 'spin ice' in a geometrically frustrated lattice of nanoscale ferromagnetic Islands, Nature (London) **439**, 303 (2006).
[5] M. Tanaka, E. Saitoh, H. Miyajima, T. Yamaoka, and Y. Iye, Magnetic interactions in a ferromagnetic honeycomb nanoscale network, Phys. Rev. B **73**, 052411 (2006).
[6] S. Zhang *et al.*, Perpendicular Magnetization and Generic Realization of the Ising Model in Artificial Spin Ice, Phys. Rev. Lett. **109**, 087201 (2012).
[7] I. A. Chioar, N. Rougemaille, A. Grimm, O. Fruchart, E. Wagner, M. Hehn, D. Lacour, F. Montaigne, and B. Canals, Nonuniversality of artificial frustrated spin systems, Phys. Rev. B **90**, 064411 (2014).
[8] U. B. Arnalds *et al.*, Thermal transitions in nano-patterned XY-magnets, Appl. Phys. Lett. **105**, 042409 (2014).
[9] R. Streubel, N. Kent, S. Dhuey, A. Scholl, S. Kevan, and P. Fischer, Spatial and temporal correlations of XY macro spins, Nano Lett. **18**, 7428 (2018).
[10] N. Leo *et al.*, Collective magnetism in an artificial 2D XY spin system, Nat. Commun. **9**, 2850 (2018).
[11] D. Louis, D. Lacour, M. Hehn, V. Lomakin, T. Hauet, and F. Montaigne, A tunable magnetic metamaterial based on the dipolar four-state Potts model, Nat. Mater. **17**, 1076 (2018).
[12] J. Sklenar, Y. Lao, A. Albrecht, J. D. Watts, C. Nisoli, G.-W. Chern, and P. Schiffer, Field-induced phase coexistence in an artificial spin ice, Nat. Phys. **15**, 191 (2019).
[13] X. Zhang, Y. Lao, J. Sklenar, N. S. Bingham, J. T. Batley, J. D. Watts, C. Nisoli, C. Leighton, and P. Schiffer, Understanding thermal annealing of artificial spin ice, APL Mater. **7**, 111112 (2019).
[14] See Supplemental Material at http://link.aps.org/supplemental/10.1103/PhysRevLett.131.126701 for descriptions of methods, additional data, and details of the analysis, which include Refs. [15–24].
[15] N. S. Bingham *et al.*, Experimental Realization of the 1D Random Field Ising Model, Phys. Rev. Lett. **127**, 207203 (2021).
[16] A. Vansteenkiste, J. Leliaert, M. Dvornik, M. Helsen, F. Garcia-Sanchez, and B. Van Waeyenberge, The design and verification of MuMax3, AIP Adv. **4**, 107133 (2014).
[17] X. Zhang *et al.*, String phase in an artificial spin ice, Nat. Commun. **12**, 6514 (2021).
[18] F. Montaigne *et al.*, Size distribution of magnetic charge domains in thermally activated but out-of-equilibrium artificial spin ice, Sci. Rep. **4**, 5702 (2014).
[19] B. Canals, I.-A. Chioar, V.-D. Nguyen, M. Hehn, D. Lacour, F. Montaigne, A. Locatelli, T. O. Menteş, B. S. Burgos, and N. Rougemaille, Fragmentation of magnetism in artificial kagome dipolar spin ice, Nat. Commun. **7**, 11446 (2016).
[20] M. E. Brooks-Bartlett, S. T. Banks, L. D. C. Jaubert, A. Harman-Clarke, and P. C. W. Holdsworth, Magnetic-Moment Fragmentation and Monopole Crystallization, Phys. Rev. X **4**, 011007 (2014).
[21] A. S. Wills, R. Ballou, and C. Lacroix, Model of localized highly frustrated ferromagnetism: The kagome spin ice, Phys. Rev. B **66**, 144407 (2002).
[22] P. Politi, M. G. Pini, and R. L. Stamps, Dipolar ground state of planar spins on triangular lattices, Phys. Rev. B **73**, 020405 (2006).
[23] P. P. Ewald, Die Berechnung Optischer Und Elektrostatischer Gitterpotentiale, Ann. Phys. (N.Y.) **369**, 253 (1921).
[24] A. Y. Toukmaji and J. A. Board Jr., Ewald summation techniques in perspective: A survey, Comput. Phys. Commun. **95**, 73 (1996).
[25] K. Machida, T. Yamamoto, T. Yamaoka, T. Ishibashi, and K. Sato, Magnetic structure of Y-shaped permalloy arrays fabricated using damascene technique, Jpn. J. Appl. Phys. **45**, L265 (2006).
[26] K. Sato, K. Machida, T. Yamamoto, T. Ishibashi, and T. Yamaoka, Magnetic characterization of regularly aligned Y-shaped permalloy arrays, J. Magn. Magn. Mater. **310**, 2342 (2007).
[27] Y. Qi, T. Brintlinger, and J. Cumings, Direct observation of the ice rule in an artificial kagome spin ice, Phys. Rev. B **77**, 094418 (2008).
[28] G. Möller and R. Moessner, Magnetic multipole analysis of kagome and artificial spin-ice dipolar arrays, Phys. Rev. B **80**, 140409 (2009).
[29] S. Zhang, I. Gilbert, C. Nisoli, G.-W. Chern, M. J. Erickson, L. O'Brien, C. Leighton, P. E. Lammert, V. H. Crespi, and P. Schiffer, Crystallites of magnetic charges in artificial spin ice, Nature (London) **500**, 553 (2013).
[30] I. A. Chioar, B. Canals, D. Lacour, M. Hehn, B. Santos Burgos, T. O. Menteş, A. Locatelli, F. Montaigne, and N. Rougemaille, Kinetic pathways to the magnetic charge

crystal in artificial dipolar spin ice, Phys. Rev. B **90**, 220407 (2014).
[31] J. Drisko, S. Daunheimer, and J. Cumings, FePd3 as a material for studying thermally active artificial spin ice systems, Phys. Rev. B **91**, 224406 (2015).
[32] K. Zeissler, S. K. Walton, S. Ladak, D. E. Read, T. Tyliszczak, L. F. Cohen, and W. R. Branford, The non-random walk of chiral magnetic charge carriers in artificial spin ice, Sci. Rep. **3**, 1 (2013).
[33] R. B. Potts, Some generalized order-disorder transformations, Math. Proc. Cambridge Philos. Soc. **48**, 106 (1952).
[34] F. Y. Wu, The Potts model, Rev. Mod. Phys. **54**, 235 (1982).
[35] F. Y. Wu, Potts model of magnetism (Invited), J. Appl. Phys. **55**, 2421 (1984).
[36] F. Graner and J. A. Glazier, Simulation of Biological Cell Sorting Using a Two-Dimensional Extended Potts Model, Phys. Rev. Lett. **69**, 2013 (1992).
[37] A. Szabó and R. M. Merks, Cellular Potts modeling of tumor growth, tumor invasion, and tumor evolution, Frontiers of Radiation Therapy and Oncology **3** (2013).
[38] J. Reichardt and S. Bornholdt, Detecting Fuzzy Community Structures in Complex Networks with a Potts Model, Phys. Rev. Lett. **93**, 218701 (2004).
[39] N. Rougemaille *et al.*, Artificial Kagome Arrays of Nanomagnets: A Frozen Dipolar Spin Ice, Phys. Rev. Lett. **106**, 057209 (2011).
[40] K. Hofhuis *et al.*, Thermally superactive artificial kagome spin ice structures obtained with the interfacial Dzyaloshinskii-Moriya interaction, Phys. Rev. B **102**, 180405 (2020).
[41] G.-W. Chern, P. Mellado, and O. Tchernyshyov, Two-Stage Ordering of Spins in Dipolar Spin Ice on the Kagome Lattice, Phys. Rev. Lett. **106**, 207202 (2011).
[42] L. Anghinolfi, H. Luetkens, J. Perron, M. G. Flokstra, O. Sendetskyi, A. Suter, T. Prokscha, P. M. Derlet, S. L. Lee, and L. J. Heyderman, Thermodynamic phase transitions in a frustrated magnetic metamaterial, Nat. Commun. **6**, 8278 (2015).
[43] N. Metropolis, A. W. Rosenbluth, M. N. Rosenbluth, A. H. Teller, and E. Teller, Equation of state calculations by fast computing machines, J. Chem. Phys. **21**, 1087 (1953).
[44] I. A. Chioar, N. Rougemaille, and B. Canals, Ground-state candidate for the classical dipolar kagome Ising antiferromagnet, Phys. Rev. B **93**, 214410 (2016).